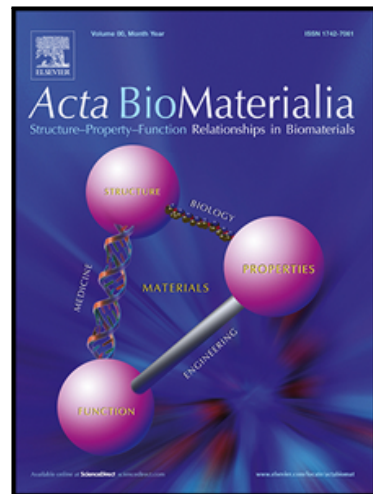


## Journal Pre-proof

Tissue expansion mitigates radiation-induced skin fibrosis in a porcine model

Laura Nunez-Alvarez, Joanna K. Ledwon, Sarah Applebaum, Bianka Progri, Tianhong Han, Joel Laudo, Vahidullah Tac, Arun K. Gosain, Adrian Buganza Tepole

PII: S1742-7061(24)00551-8  
DOI: <https://doi.org/10.1016/j.actbio.2024.09.035>  
Reference: ACTBIO 9555



To appear in: *Acta Biomaterialia*

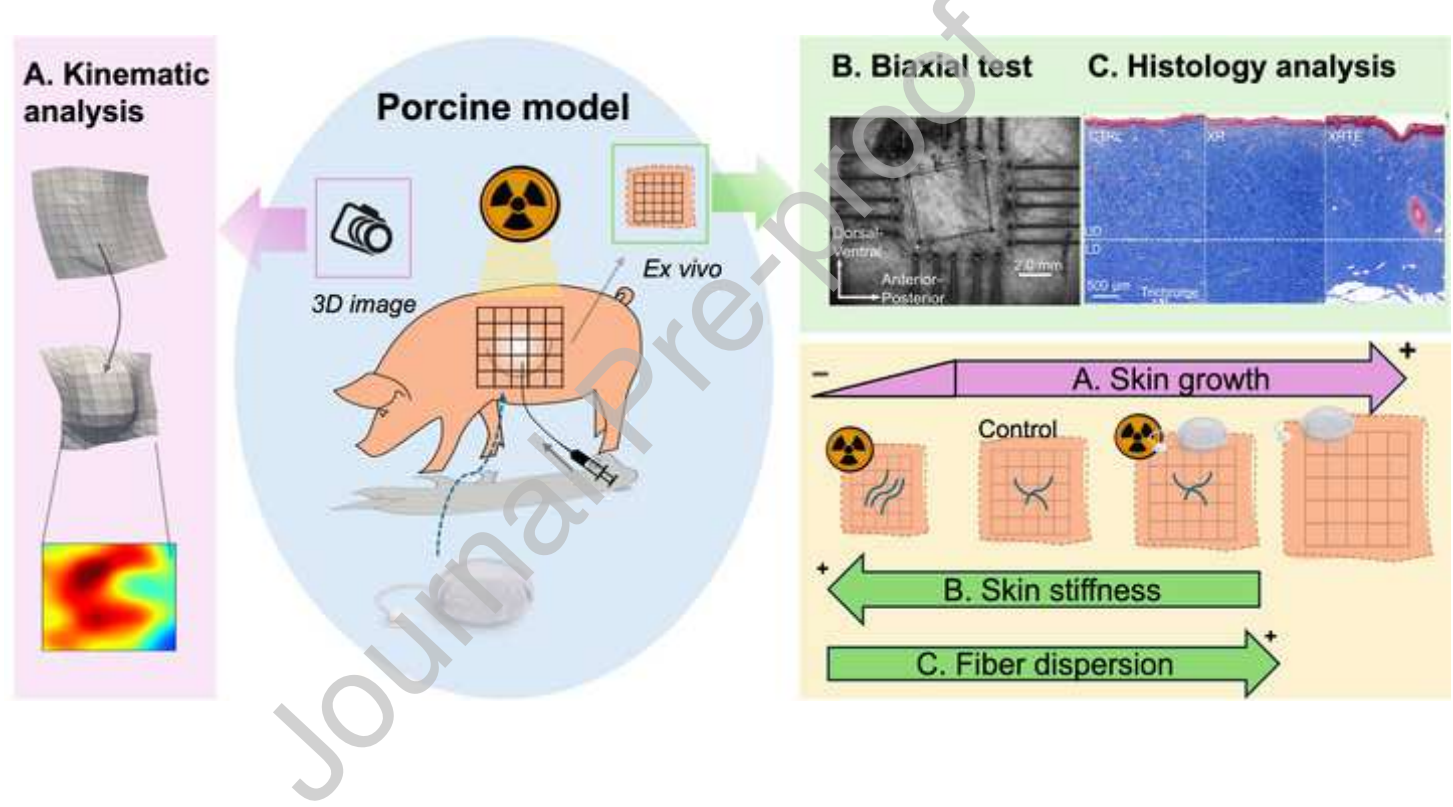
Received date: 29 March 2024  
Revised date: 13 September 2024  
Accepted date: 19 September 2024

Please cite this article as: Laura Nunez-Alvarez, Joanna K. Ledwon, Sarah Applebaum, Bianka Progri, Tianhong Han, Joel Laudo, Vahidullah Tac, Arun K. Gosain, Adrian Buganza Tepole, Tissue expansion mitigates radiation-induced skin fibrosis in a porcine model, *Acta Biomaterialia* (2024), doi: <https://doi.org/10.1016/j.actbio.2024.09.035>

This is a PDF file of an article that has undergone enhancements after acceptance, such as the addition of a cover page and metadata, and formatting for readability, but it is not yet the definitive version of record. This version will undergo additional copyediting, typesetting and review before it is published in its final form, but we are providing this version to give early visibility of the article. Please note that, during the production process, errors may be discovered which could affect the content, and all legal disclaimers that apply to the journal pertain.

© 2024 Published by Elsevier Ltd on behalf of Acta Materialia Inc.

Graphical Abstract



# Tissue expansion mitigates radiation-induced skin fibrosis in a porcine model

Laura Nunez-Alvarez<sup>a</sup>, Joanna K. Ledwon<sup>b</sup>, Sarah Applebaum<sup>b</sup>, Bianka Progri<sup>b</sup>, Tianhong Han<sup>c</sup>, Joel Laudo<sup>c</sup>, Vahidullah Tac<sup>c</sup>, Arun K. Gosain<sup>b,d</sup>, Adrian Buganza Tepole<sup>a,c,\*</sup>

<sup>a</sup>*Weldon School of Biomedical Engineering, Purdue University*

<sup>b</sup>*Lurie Children's Hospital*

<sup>c</sup>*School of Mechanical Engineering, Purdue University*

<sup>d</sup>*Department of Plastic and Reconstructive Surgery, Northwestern School of Medicine*

## Abstract

Tissue expansion (TE) is the primary method for breast reconstruction after mastectomy. In many cases, mastectomy patients undergo radiation treatment (XR). Radiation is known to induce skin fibrosis and is one of the main causes for complications during post-mastectomy breast reconstruction. TE, on the other hand, induces a pro-regenerative response that culminates in growth of new skin. However, the combined effect of XR and TE on skin mechanics is unknown. Here we used the porcine model of TE to study the effect of radiation on skin fibrosis through biaxial testing, histological analysis, and kinematic analysis of skin deformation over time. We found that XR leads to stiffening of skin compared to control based on a shift in the transition stretch (transition between a low stiffness and an exponential stress-strain region characteristic of collagenous tissue). The change in transition stretch can be explained by thicker, more aligned collagen fiber bundles measured in histology images. Skin subjected to both XR+TE showed similar microstructure to controls as well as similar biaxial response, suggesting that physiological remodeling of collagen induced by TE partially counteracts pro-fibrotic XR effects. Skin growth was indirectly assessed with a kinematic approach that quantified increase in permanent area changes without reduction in thickness, suggesting production of new tissue driven by TE even in the presence of radiation treatment. Future work will focus on the detailed biological mechanisms by which TE counteracts radiation induced fibrosis.

## Introduction

Breast cancer is the predominant new cancer diagnosis in women and the second leading cause of cancer-related mortality in the United States [1]. Approximately half of U.S. women with breast cancer opt for mastectomy and over 40% of those undergo reconstruction based on tissue expansion (TE) [2]. TE is the process of inserting a balloon-like device under the skin and gradually inflating it to promote skin growth [3, 4]. Post-mastectomy radiation therapy (PMRT)

\*Corresponding author  
Email: abuganza@purdue.edu

is administered depending on the severity of the disease. For patients with stage I or II breast cancer, 49% undergo breast conserving surgery (BCS) with radiation, while 5% undergo mastectomy and radiation. In contrast, for patients with stage III, 45% undergo mastectomy and radiation and 16% undergo BCS and radiation [5].

<sup>10</sup> Stretch is known to trigger mechanoresponsive pathways in skin cells via mechanoreceptors that govern cell proliferation and collagen production [6, 7]. Radiation, in contrast, leads to tissue damage and complications such as tissue necrosis and radiation-induced fibrosis (RIF) [8, 9]. Yet, the influence of radiation on collagen alterations in the presence of TE-induced growth remains unknown [10]. As a result, there is controversy regarding the optimal timing of <sup>15</sup> radiation and TE [11].

<sup>20</sup> Due to its positive effect on quality of life for breast cancer survivors, immediate breast reconstruction is usually recommended [12, 13]. However, when PMRT is needed, there is no consensus whether TE should occur before, during, or after radiation therapy [11, 14, 15]. On the one hand, radiation to the expander has been reported to cause complication rates requiring re-operation between 4.8% and 40% [16, 17, 9]. In contrast, radiation to the permanent implant (after breast reconstruction is complete), does not lead to major complications, but often leads to tissue contracture and capsule formation with negative aesthetic outcomes: 50% incidence when the implant is radiated compared to 17% when PMRT is administered to the expander[16, 18]. <sup>25</sup> In delayed reconstruction, PMRT is administered to the expander, followed by 4-6 months gap before the final reconstructive surgery of the breast [14]. An intermediate approach known as delayed-immediate breast reconstruction is to insert an expander, administer PMRT, wait two or more weeks to resume TE, then wait three or more months for final reconstructive surgery [14, 19]. Despite the lack of consensus, recent trends show a steady increase in patients <sup>30</sup> receiving immediate breast reconstruction ( $\approx$  50%) or delayed-immediate reconstruction ( $\approx$  30%) [15, 20]. Understanding the interplay between radiation, tissue expansion, and skin fibrosis is crucial to reduce complication rates and improve cosmetic outcomes.

<sup>35</sup> X-ray exposure initiates cytokine cascades and fibro-inflammatory pathways, leading to RIF over prolonged periods of time [21, 22]. Radiation leads to production of reactive oxygen species (ROS) and damage-associated molecular patterns (DAMPs), which induce release of various cytokines that eventually lead to recruitment of inflammatory cells [23]. Transforming growth factor beta (TGF $\beta$ ) secreted by macrophages prompts fibroblasts to differentiate into myofibroblasts, driving excessive extracellular matrix (ECM) synthesis and fibrotic tissue formation [24]. Radiation can also directly impact collagen architecture, via molecular <sup>40</sup> cross-linking and dermal remodeling even as early as 24 hours after a 2 Gy irradiation dose [25, 26]. Furthermore, radiation has been linked to a reduction in collagen ultimate strain (strain at failure) while at the same time increasing collagen stiffness [25]. However, a comprehensive understanding of collagen changes upon radiation is still lacking. Moreover, during TE, additional collagen remodeling exists, which is likely to influence RIF, but this remains <sup>45</sup> unknown.

TE induces temporary hypoxia and ischemia, leading to the production of hypoxia-related chemokines that contribute to mechanoresponsive pathway activation [27], promoting cell proliferation for tissue regeneration (vascular growth or angiogenesis in the dermis as well as keratinocyte proliferation in the epidermis) [28, 7]. However, the co-regulation of inflammatory <sup>50</sup> as well as pro-regenerative pathways through expansion and radiation remains poorly understood. Moreover, there is a dearth of research characterizing the role of TE in mitigating or aggravating radiation-induced mechanical changes in the skin, such as RIF.

In this study, we chose mini-Yucatan pigs as research subjects for TE and radiation due to their

similar attributes with human skin, which include epidermis and dermis thickness [29], tight skin-subcutaneous tissue connection (unlike rodents) [30], and shared gross, microscopic, and ultra-structural features [31], resulting in a comparable mechanical and structural response. Here, we analyze the skin mechanical behavior under TE and radiation, alongside examining collagen structural changes and their impact on skin growth.

## Materials and Methods

### *Porcine model*

Five 2-month-old female Yucatan minipigs were used for the study (Premier BioSource). The protocols follow closely our previous work [32, 33]. Four  $10 \times 10 \text{ cm}^2$  grids were tattooed on their backs, and 100 mL tissue expanders (Mentor) were inserted underneath the grids, in four of the individuals **seven days after tattooing** (Fig. 1A). On the fifth pig, just two grids without expanders were analyzed. For the first three animals, **seven days after placement**, the expanders were filled with 45 cc of a normal saline solution and, seven days later, were filled again with the same volume for a total final volume of 90cc. For the fourth animal, the resident in charge noted excessive deformation of the skin that could compromise viability of the tissue and two 30cc inflations were done instead for a total of 60 cc with otherwise the same timing. In addition to tattooed grids, skin patches adjacent to the grids were collected to serve as controls or to understand the effect of radiation without tissue expansion (Fig. 1B). **Radiation dose was supplied six days after second inflation** Some of the expanded grids were used to understand the effect of biological cover [32] and were excluded from this study. Out of a total of 20 patches available for this study, 11 were exposed to radiation: four on the first pig, two on the left side of each of the second, third, and fourth pigs, and one on the fifth pig.

The radiotherapy protocol was developed based on a plaster mold of the targeted radiation area after the second inflation. The mold was CT scanned to determine the geometry of the expanded skin. Northwestern University Department of Radiation Oncology regularly creates radiation plans for human breast cancer patients and they created the plans for the pigs in this study based on the CT scan of the mold. The animal study protocol was approved by the Institutional Animal Care and Use Committee of Northwestern University (protocol number IS00010747, 7/31/2019). On the day of radiation, the anesthetized animal was positioned and immobilized in the same manner as during the CT simulation. The animal received a single fraction of 20 Gy [34, 35], employing megavoltage photon beam energies (610 MV). The beams were arranged at two oblique gantry angles, maintaining a standard 100 cm source-to-axis distance on an Elekta Infinity system.

The radiation protocol was based on established protocols from the literature [36, 35, 34], as well as our prior studies [32]. A single fraction of 20 Gy approximates the effects of radiation given in PMRT and has been well tolerated in a porcine model [36, 32, 35]. Tissue collection at 8 weeks post-radiation allows for evaluation of late effects of radiation [37, 26]. In animals two to five, only the left side was radiated. The rationale is that side (left or right) is not expected to have an effect [38] Moreover, maintaining the left side allowed for a more repeatable radiation protocol across the animals.

We analyzed four expanded radiated patches (one from each of the first four pigs), six radiated patches (two from the first pig, one each of the other four pigs), six control non-radiated patches (one each from the second to fifth pigs, two more from non-radiated pigs that were not part of this particular study but rather prior work [39]) and one expanded patch from the second pig.

With these settings we were able to collect radiated skin (XR), expanded (TE), expanded and radiated (XRTE), and control (CTRL) (Fig. 1B). All patches were collected after 8 weeks of radiation. For this study, we performed mechanical testing under biaxial stretching conditions. While the original study design incorporated two grids involving TE without radiation, one of the expanders leaked, which made a thorough comparison difficult. Consequently, these results were mostly excluded from the study (except from the kinematic analysis of skin growth). Nonetheless, the analyzed patches enabled a direct comparison between the CTRL, XR, and 105 XRTE protocols.

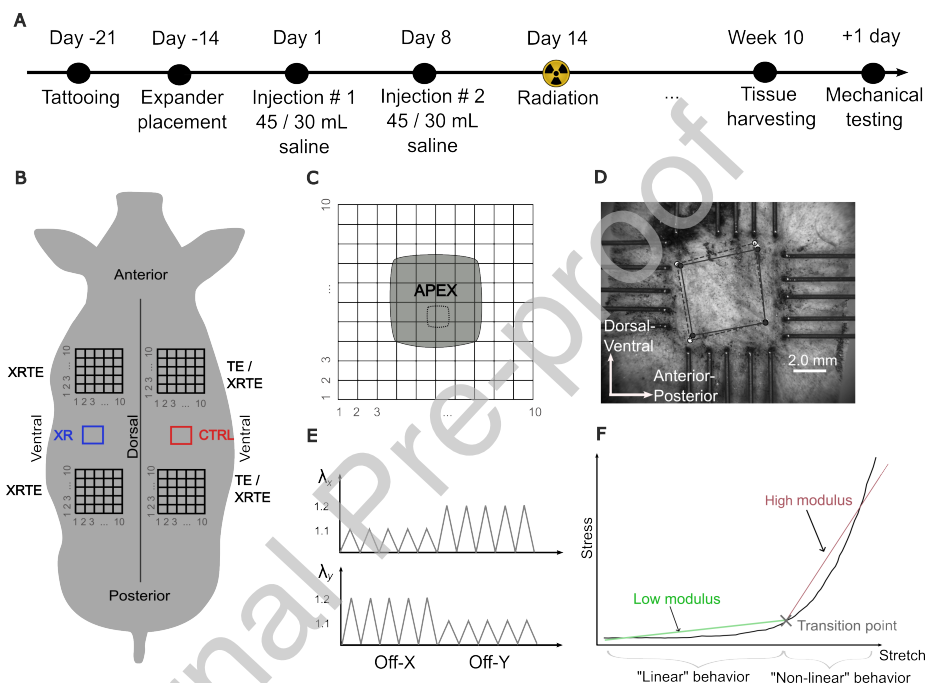


Figure 1: Porcine model. **A)** Timeline of the animal model. **B)** Four tattooed grids on the back of Yucatan minipigs were assigned either control (CTRL), radiation (XRT), radiated and expanded (XRTE), or expander protocols without radiation (TE). For the expanded patches, rectangular expanders were inflated to 90 mL in two inflation steps 7 days apart except for one pig which received 60cc inflation due to concerns of excessive deformation. **C)** At the end of 10 weeks (8 weeks after radiation), patches were excised and the apex was collected for biaxial mechanical testing (**D**). **E)** Biaxial testing consisted of cyclic loading, 5 cycles of off-x biaxial deformation (greater stretch in y) followed by 5 cycles of off-y deformation. **F)** A representative stress-strain loading curve shows a linear part of the curve followed by strain stiffening in a non-linear manner. Tangent modulus for the low stiffness and high stiffness regions were determined, as well as the transition stretch.

### Mechanical testing

Freshly excised skin from the grids was prepared by removing subcutaneous tissue and cut into  $7 \times 7 \text{ mm}^2$  samples. These samples were collected from the central area of the grid, which aligns with the apex region of the expander (which undergoes the greatest amount of stretch and growth), see Fig. 1C. The sample thickness was measured with a thickness gauge and then mounted on the CellScale Biostester (CellScale, Waterloo, Canada), under physiological conditions ( $37^\circ\text{C}$  water bath) with a preload of 50 mN, as described in [40]. Force data were 110

collected along with images from which the displacement was tracked using the digital image correlation software DICe (Fig. 1D). Here, dorsal-ventral direction was kept consistent as the Y axis and anterior-posterior as the X axis.

115

Two different cyclic loading conditions were used. First, five cycles of Off-X loading corresponding to  $\lambda_x = 1.1, \lambda_y = 1.2$ , followed by five cycles of Off-Y biaxial loading to stretches  $\lambda_x = 1.1, \lambda_y = 1.2$ . (Fig. 1E). These deformations were selected based on our previous work showing they can accurately capture the anisotropic response of skin [41, 40]. Strain rate used was  $\dot{\lambda} = \lambda_{max}/20s^{-1}$ . After processing the data collected with the measured thickness of the skin, along with the force and displacement from these mechanical tests, nominal stress-stretch curves were obtained. The mechanical response reported in these curves shows an initial linear behavior that is related to the reorganization and straightening of the collagen fibers and a second stage of non-linear behavior governed by the tensile response of such fibers embedded in the ECM [42]. Several parameters were computed from the stress-stretch data: from the linear behavior, the *low modulus* was defined as the slope of that part of the curve, and, similarly, the *high modulus* was defined for the non-linear portion of the curve. The point that divides both stages is the *transition stretch* (Fig. 1F). The corresponding *transition stress* was also extracted from the data. *to compute the transition stretch we first smooth the data with the savgol filter from the Signal module of the Scipy library in Python. Then, for every point in the stress-stretch curve we do linear regression and obtain the slope around a neighborhood of a point. Several options were tried but we settled on three points, equivalent to a central difference scheme. Lastly, we compute the gradient of the slopes vector to find the location of maximum slope change and we use this stretch as the transition point. The code is available in the Github repository listed at the end of the article.*

120

125

130

135

#### *Constitutive modeling of skin*

Skin was assumed hyperelastic and described with the Gasser-Ogden-Holzapfel (GOH) material model with two fiber families [43, 44]. Namely, the strain energy takes the form

$$\Psi = \frac{\mu}{2}(I_1 - 3) + \sum_{i=1}^2 \frac{k_{1i}}{2k_{2i}} [e^{(k_{2i}[\kappa_i I_1 + (1-3\kappa_i)I_{4i}-1]^2)} - 1] + p(1-J) \quad (1)$$

140

145

where the first term is an isotropic neo-Hookean contribution, the second term accounts for the exponential fiber response, and the last term is to ensure incompressibility through the Lagrange multiplier pressure  $p$ . The neo-Hookean part is parameterized by the shear modulus  $\mu$  and it depends on the first invariant  $I_1 = \text{tr}(\mathbf{C})$  of the right Cauchy Green deformation tensor  $\mathbf{C}$ . The fiber part introduces parameters  $k_1, k_2$ , and  $\kappa$ , and depends on the fourth pseudo-invariant  $I_4 = \mathbf{C} : \mathbf{M} = \mathbf{C} : \mathbf{a}_0 \otimes \mathbf{a}_0$  where  $\mathbf{a}_0$  is the preferred fiber direction. Two fiber families were considered. Second Piola Kirchhoff stress for this strain energy is

$$\mathbf{S} = -p\mathbf{C}^{-1} + \mu\mathbf{I} + \sum_{i=1}^2 2k_{1i}E_{fi}e^{k_{2i}E_{fi}^2} [\kappa_i\mathbf{I} + (1-3\kappa_i)\mathbf{M}_i] \quad (2)$$

where we have introduced the fiber strain  $E_f = \kappa I_1 + (1-3\kappa)I_4 - 1$  for a more concise notation.

Again, note that two fiber families were considered in Eq. (2). Other stress tensors such as Cauchy stress  $\boldsymbol{\sigma}$ , or first Piola Kirchhoff (nominal) stress  $\mathbf{P}$  can be readily obtained from  $\mathbf{S}$  using

the deformation gradient  $\mathbf{F}$  [43]. The rationale for the model GOH with two fiber families comes from our previous work on imaging collagen microstructure on porcine dermis [38], and extensive literature showing bi-modal fiber distribution of collagen fiber orientation in the back of rats, mice, pigs and humans [45, 46, 47, 48]. Other constitutive models appropriate for skin are reviewed in [49], with more detailed microstructure models achieving higher accuracy but at the expense of a greater number of parameters [47, 50, 51]. The GOH model offers a good balance between accuracy and number of parameters [41].

155

#### *Bayesian estimation of model parameters*

A hierarchical Bayesian framework was used to estimate the parameters of the GOH model, similar to our previous work [52]. Briefly, a full covariance matrix  $\mathbf{K}^{\text{params}}$  of dimension  $n_p \times n_p$ ,  $n_p$  the number of parameters, is used as a hyper-prior by first sampling  $\mathbf{L} \in \mathbb{R}^{n_p} \times \mathbb{R}^{n_p}$ ,  $L_{ij} \sim N(0, 1)$  and then assigning  $\mathbf{K}^{\text{params}} = \mathbf{L}\mathbf{L}^T$  such that it is symmetric positive semi-definite.

A hyper-prior for the mean vector of parameters is also sampled  $\boldsymbol{\mu}^{\text{params}} \in \mathbb{R}^{n_p}$ ,  $\boldsymbol{\mu}_i^{\text{params}} \sim N(0, 1)$ . Then, for every tissue specimen tested ( $i$ ), individual parameter realizations are drawn from the multi-variate Gaussian  $\mathbf{k}^{(i)} \sim \mathcal{N}(\mathbf{k}|\boldsymbol{\mu}^{\text{params}}, \mathbf{K}^{\text{params}})$ , where the vector  $\mathbf{k} = [\mu, k_{1,1}, k_{2,1}, \kappa_1, k_{1,2}, k_{2,2}, \kappa_2]$  is the vector of parameters to be calibrated, namely the shear modulus of the isotropic part, and the fiber parameters for the two fiber families. Given a realization of parameters for an individual specimen  $\mathbf{k}^{(i)}$ , the first Piola Kirchhoff stress under biaxial loading  $\mathbf{P}_{\text{pred}}^{(i)}$  is computed with the model 2, and compared to the experimentally observed stress  $\mathbf{P}_{\text{exp}}^{(i)}$  using a Gaussian likelihood with prior noise variance  $\sigma_m \sim \text{Half - Normal}(0.005)$ . Markov chain Monte Carlo sampling is used with the Python package NumPyro [53]. Posterior traces of 2000 samples are generated after 2000 warm-up samples with the NUTS sampling scheme.

165

170

#### *Collagen histological analysis*

Histology images of biopsies taken from the pig transverse plane (through the thickness rather than parallel to the skin surface) of the three different skin groups were stained with Masson's Trichrome stain in which collagen is shown in blue and epithelial cells in red. Using the OrientationJ plugin within ImageJ, we analyzed the *orientation distribution* of collagen fibers in each sample. This involved calculating the local pixel structure tensor  $J_p$ , derived from the spatial derivatives of intensity within the region of interest (ROI). The eigenvalues and eigenvectors of  $J_p$  can be defined as  $\lambda_{\max}^{\text{img}}$ ,  $\lambda_{\min}^{\text{img}}$  and  $\mathbf{v}_{\max}^{\text{img}}$ ,  $\mathbf{v}_{\min}^{\text{img}}$ , respectively. The direction of the largest tensor eigenvector  $\mathbf{v}_{\max}^{\text{img}}$  corresponds to the local predominant orientation [54]. Thus, by analyzing the frequency of these local values across the entire ROI, we can determine the orientation distribution of collagen fibers. Notably, this analysis was specifically conducted on the blue channel, representing collagen within the entire dermal region.

185

190

In addition to orientation distribution, OrientationJ allows for quantification of the strength of collagen alignment in a given region, termed *coherency*. The coherency value is based on the ratio  $(\lambda_{\max}^{\text{img}} - \lambda_{\min}^{\text{img}})/(\lambda_{\max}^{\text{img}} + \lambda_{\min}^{\text{img}})$ . A coherency of 1 indicates perfectly aligned fiber while a value of 0 indicates dispersed fibers. For the coherency study, we considered around 25 analysis windows per sample. This number of regions was selected to minimize noise but retain spatial resolution as suggested in [55].

### Statistical analysis

We conducted statistical analyses to compare between groups. Initially, we assessed homoscedasticity using Bartlett's test. If the data met this condition, we proceeded with an ANOVA followed by a Bonferroni post hoc test. Alternatively, if homoscedasticity was not met, we performed the non-parametric Kruskal-Wallis test followed by a Dunn's multiple comparisons test to assess pairwise significance. For comparisons involving orientation distributions, we computed the average distribution for each group and performed pairwise comparisons using the Kolmogorov-Smirnov test. Throughout all analyses, a significance level of 0.05 was considered.

### Isogeometric analysis of surface deformation and growth

We also analyzed the deformation of the grid based on prior work. Namely we took 3D photographs of tattooed grids on the back of the animals before inflation, then after inflation, then at the end of the 10 weeks, before and after animal sacrifice. 3D photos were collected with the Vectra H2 system (Canfield, Parsippany, NJ, USA). The 3D surfaces (\*obj) were converted into NURBS surface patches and analyzed with our previously published code [33]. Comparison between grids is possible because the same NURBS parameterization is used for the tattooed grids across all time points and the initial grids are all  $10 \times 10\text{cm}^2$ . There is no need for the surfaces to share the same coordinate system [56]. The surface deformation gradient from *in vivo* pre-expansion up to the point before animal sacrifice is denoted  $\mathbf{F}$ . After excision we have the elastic deformation is  $\mathbf{F}^e$ . From previous work we also know the pre-strain  $\mathbf{F}^p$ , i.e. the natural elastic deformation of skin *in vivo*. Tissue growth can be calculated from  $\mathbf{FF}^p = \mathbf{F}^e\mathbf{F}^g$ . Alternatively, we work with the area changes  $\vartheta = \det \mathbf{F}_s$  where  $\mathbf{F}_s$  denotes the surface deformation (ignoring thickness strains). The multiplicative relationship of the total, elastic, pre-strain and growth deformations applies to the area changes:  $\vartheta\vartheta^p = \vartheta^e\vartheta^g$ . We did the analysis for three expanded radiated patches (XRTE). We also had one single patch for which we had a TE treatment with no radiation. Unfortunately, only one patch of the TE cases was processed because the other repeat of that condition failed due to expander leak.

## Results

### Mechanical response of skin

Skin average thickness from the three groups is shown in Table 1. No significance between groups were found. Nonetheless, the XR skin tended to be thicker compared to CTRL and XRTE. The biaxial tests were analyzed as illustrated in Fig. 1 to quantify the features of the stress-stretch response in terms of low and high modulus, and the transition stretch and stress between the linear and nonlinear regions. The results of this analysis are depicted in Fig. 2. In general, the dorsal-ventral direction reaches highest stresses because this direction coincides with Langer lines in the dorsal skin of the swine [57]; Langer lines being associated with preferred collagen orientation and anisotropy direction for the tissue [45]. There is no

Table 1: Thickness of excised skin samples prior to biaxial testing.

Group	Mean [mm]	std
CTRL	2.061	0.613
XR	2.367	0.318
XRTE	2.030	0.064

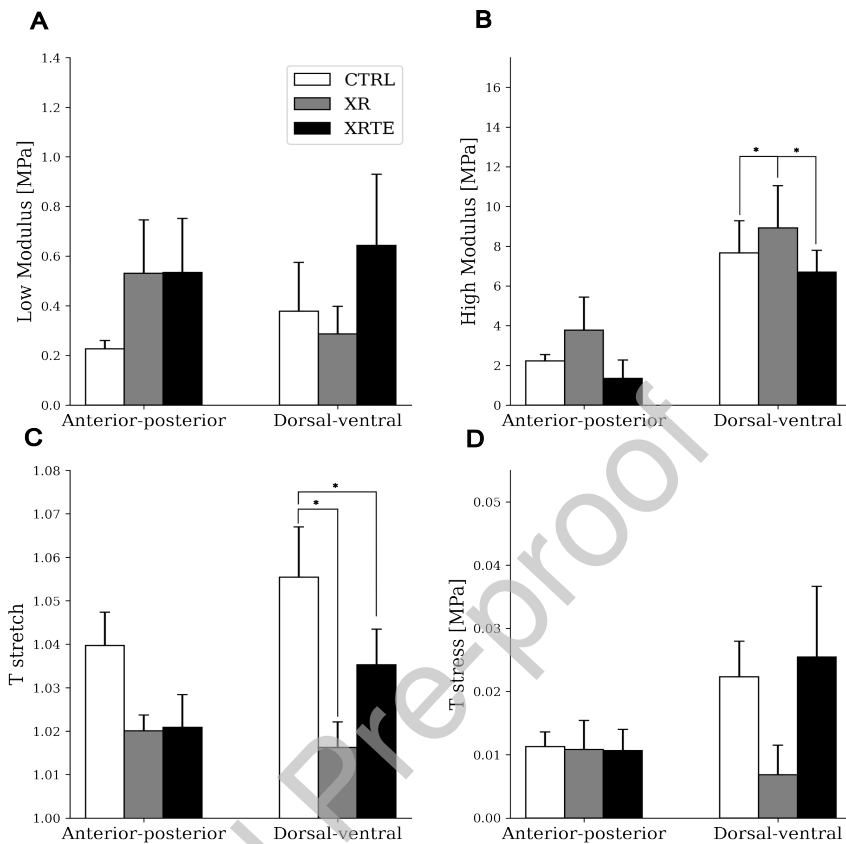


Figure 2: Mechanical test metrics: A) *Low Modulus*, no significance found between groups in any direction B) *High Modulus*, XR skin showed the highest modulus at large stretch values in the dorsal-ventral direction compared to both CTRL and XRTE (\* $p < 0.05$ ). C) *Transition stretch* was significantly lower in XR and XRTE cases compared to CTRL in the dorsal-ventral region (\* $p < 0.05$ ), D) *Transition stress*, was not significantly different.

statistically significant change in the low modulus of XR or XRTE when compared to CTRL (Fig. 2A). However, radiation tends to increase the low modulus compared to controls. The 230 high modulus on the other hand (Fig. 2B), shows a clear trend in both directions, with statistical significance in the dorsal-ventral direction which is associated with the main fiber orientation. XR skin was stiffer in the dorsal-ventral direction when compared to CTRL skin ( $p=0.008$ ), and XRTE group showed significantly less stiffness when compared to XR skin ( $p=0.016$ ). Visually, and according to the literature [21], the radiated skin does look unhealthy and stiffer 235 than the controls.

A similar change in skin stiffness trend is shown with the transition stretch (Fig. 2C). The XR skin has a much smaller transition stretch in the dorsal-ventral direction compared to CTRL skin ( $p=0.016$ ), revealing that radiated skin, upon stretch, quickly goes into the nonlinear region. In other words, radiated skin has lost the initial low stiffness region characteristic of healthy skin [58]. Interestingly, the XRTE group recovered partially the transition stretch, yet, it 240

was still significantly lower than the controls ( $p=0.033$ ), suggesting that collagen reorganization due to tissue expansion partially restores the initial low stiffness region but not completely. No statistically significant changes were observed in the transition stresses. Overall, these results corroborate that radiation on doses similar to those used clinically lead to skin fibrosis, but these effects are partially mitigated by tissue expansion.

245

### Bayesian calibration

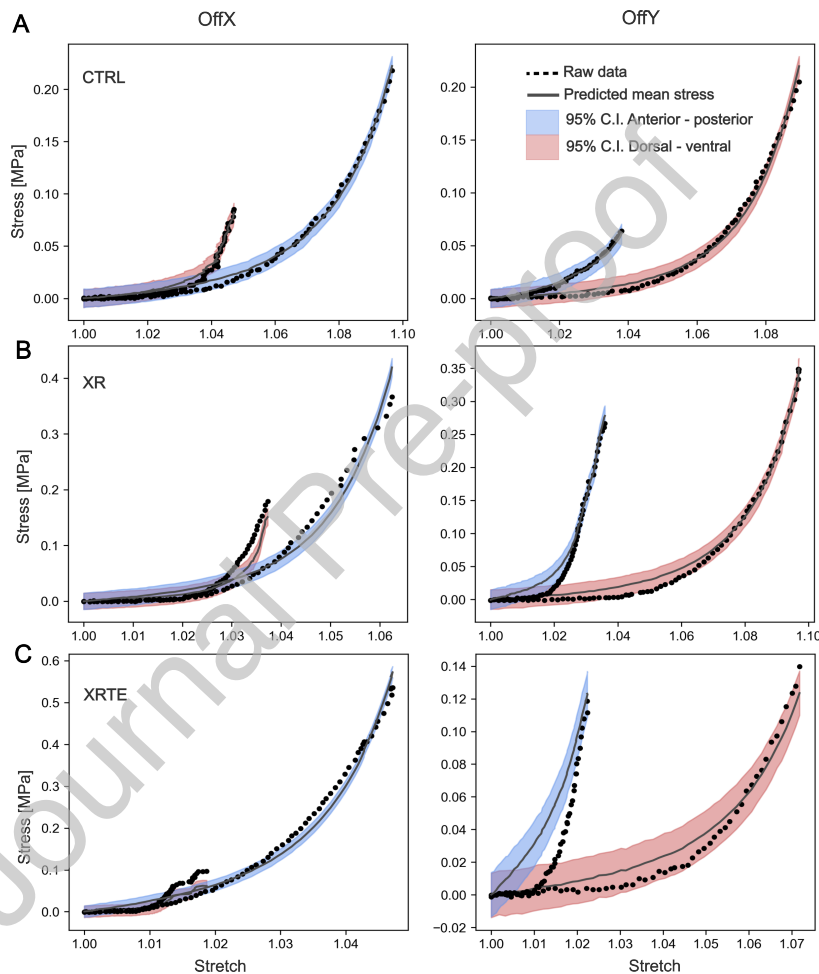


Figure 3: Bayesian calibration results. Representative posterior predictions for one of the samples of each A) CTRL, B) XR, C) XRTE cases for both off-biaxial x and off-biaxial y deformations.

The hierarchical Bayesian calibration method leads to posterior predictive distributions for the parameters of the GOH model Eq. (2). Fig. 3 shows the posterior predictive stress-stretch curves for the three cases of interest for one sample each of CTRL, XR, XRTE. The plots show mean prediction and 95% confidence interval. The GOH model is able to adequately capture the experimental data. Note that the calibration leads to distribution of the parameters for both

Table 2: GOH model fit to individual skin samples using the hierarchical Bayesian framework.

Group	$\mu$	$k_{1,1}$	$k_{2,1}$	$\kappa_1$	$\alpha_1$	$k_{1,2}$	$k_{2,2}$	$\kappa_2$	$\alpha_2$
CTRL	9.36E-04	8.26E-02	2.55E+02	2.48E-04	1.06E+00	9.66E-03	2.06E+02	5.90E-08	-2.67E+00
CTRL	1.19E-04	7.84E-01	3.24E+02	2.44E-01	1.52E+00	5.94E-01	4.57E+02	2.39E-01	-3.23E+00
CTRL	2.43E-02	1.16E-02	1.40E+02	1.57E-07	4.79E-01	5.29E-03	4.45E+01	1.10E-06	1.76E+00
CTRL	4.40E-04	4.14E-03	8.31E+01	1.97E-07	-9.57E-01	1.03E-02	1.98E+02	3.63E-05	2.07E+00
CTRL	3.71E-04	1.46E-01	2.53E+02	9.22E-04	-9.67E-01	3.89E-02	1.28E+02	2.18E-02	5.07E-05
CTRL	1.32E-04	1.15E-02	7.85E+01	4.10E-04	7.89E-01	4.00E-03	1.33E+02	2.40E-02	-2.39E+00
XR	2.80E-04	5.20E-02	2.85E+01	1.00E-05	-3.19E+00	1.79E-01	2.03E+02	8.34E-03	2.11E+00
XR	9.40E-06	8.18E-02	5.47E+01	5.65E-05	1.60E+00	1.31E-01	2.56E+02	5.34E-06	7.34E-01
XR	1.04E-04	1.81E-01	5.29E+02	2.59E-02	1.14E+00	2.54E-02	3.57E+02	1.28E-02	-4.17E-01
XR	1.41E-06	2.46E-01	1.64E+02	1.86E-05	1.03E+00	4.35E-02	6.20E+01	7.18E-03	4.66E-02
XR	1.01E-06	3.37E-02	6.18E+01	1.26E-06	-1.63E+00	6.12E-03	2.29E+02	7.22E-05	7.08E-01
XR	3.87E-04	4.37E-02	9.92E+01	8.33E-05	-2.17E+00	1.70E-04	3.49E+02	4.04E-02	-4.62E-01
XRTE	4.94E-03	9.45E+01	6.61E+01	3.23E-01	-4.15E+00	1.04E+00	8.36E+02	9.21E-03	-1.15E+00
XRTE	8.57E-05	6.62E-01	1.91E+02	1.30E-04	1.89E+00	7.08E-02	7.91E+01	1.14E-02	-9.96E-02
XRTE	1.82E-02	1.63E-02	1.04E+02	9.33E-05	1.34E+00	8.85E-06	6.68E+02	1.40E-03	-1.59E+00
XRTE	2.40E-02	1.61E-03	7.95E+02	3.93E-07	-1.56E+00	1.11E-03	7.72E-01	3.29E-01	5.39E+00

individual samples as well as the entire population. The calibration code and raw data is provided through a Github repository at the end of the article. Table 2 contains the summary of the parameters. Because of the wide ranges of the parameters after the calibration, it was not possible to determine significant differences in the parameters. Nevertheless, the individual fits are important for predictive simulations of radiated skin. From the stress-stretch data in Fig. 3 it can be qualitatively observed that radiated skin reaches much higher values of stress at smaller deformations, i.e. radiated skin is stiffer than controls.

#### Collagen analysis

Fibers of XR skin tend to re-accommodate in bundles and appear less dispersed than controls, whereas in XRTE skin, fibers appear more dispersed than XR (Fig. 4 A-B). Many of the fiber orientation distributions have two modes (Fig. 4C). When computing the orientation distribution of all the biopsies taken and comparing pairwise between the average curve of the groups using Kolmogorov-Smirnov test, we found significant difference between CTRL XR, CTRL - XRTE and XR XRTE ( $p < 0.001$  for the three cases). In the combined plot CTRL and XRTE skin have similar dispersion and mode values. On the other hand, XR skin is less dispersed. Another analysis computed with ImageJ was the coherency analysis that considered several regions of interest (ROIs) on each histological image (Fig. 4D) in which an upper (2/3 of the thickness) and lower region were defined (1/3 of the thickness), corresponding to papillary and reticular dermis.

To carry on the coherency analysis, three biopsies were taken per patch, four patches per group ( $n = 12$ ). A minimum of 2 non-consecutive sections per biopsy were analyzed ( $n > 24$ ). On each section, around 25 and 10 ROIs were analyzed for both upper and lower dermis, respectively, and averaged among sections, biopsies and individuals, to have a representative value per group and compare between them. In the upper dermis (UD), XRTE showed the highest coherency value, followed by XR group and finally CTRL group. Conversely, in the lower dermis (LD), XRTE skin showed a significantly lower coherency when compared to XR and CTRL ( $p < 0.001$ ) which is a similar result to our previous study of TE [59]. There is also significant difference between CTRL-XR ( $p < 0.001$ ), with CTRL skin showing the lowest coherency in both the upper and lower dermis. The difference between the XR and XRTE at the UD region might be mediated by the way different radiation doses interact with the tissue at different depths, as well as coupling between epidermis-dermis signaling [24, 60].

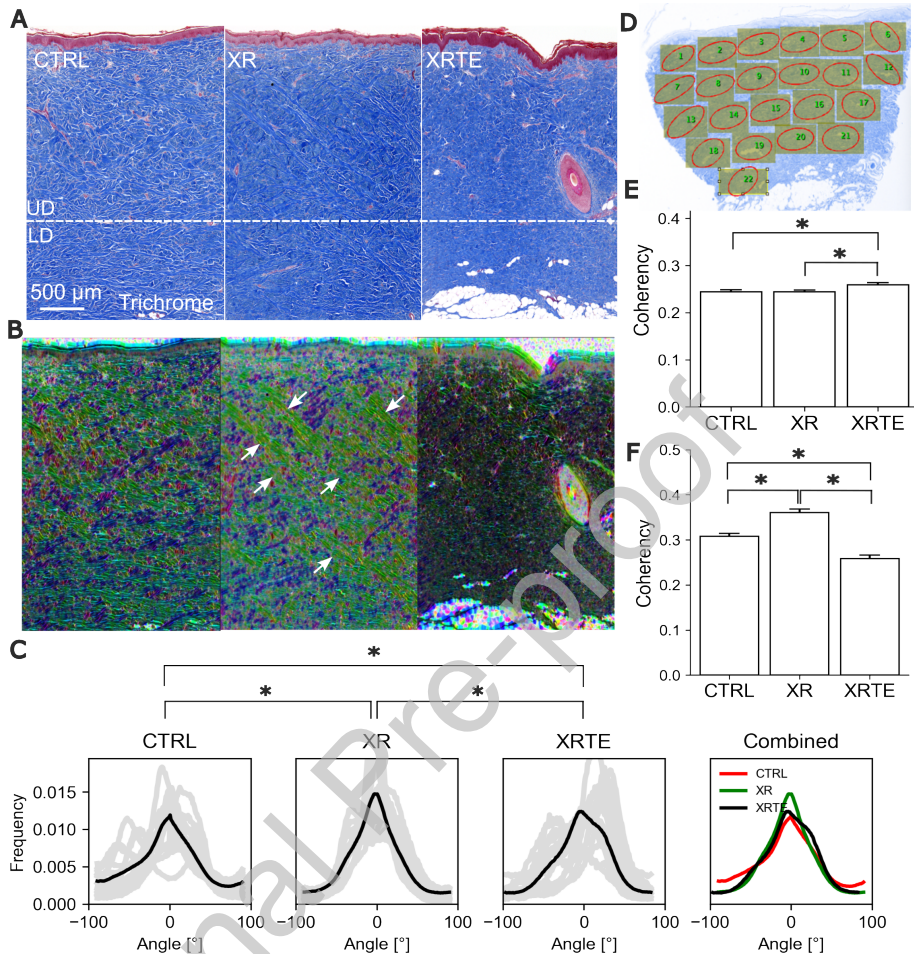


Figure 4: Collagen analysis. A) Mason's trichrome stained histology slices in the transverse plane of the CTRL, XR, XRTE cases. The white dotted line divides the dermis into a top region or Upper Dermis (UD) and bottom region or Lower Dermis (LD). The first one is defined as the initial two thirds of the dermis thickness. B) Analysis with the OrientationJ plug-in computes the alignment of the fibers (blue channel). C) In the transverse plane, collagen is expected to have a basket weave arrangement with two modes and significant dispersion captures in the probability density functions of CTRL, XR, XRTE. Comparison of the probability densities with the Kolmogorov-Smirnov showed difference between the three groups. D) In addition to orientation, regions of interest (ROI) were selected for coherency analysis, which measures the strength of the alignment. Coherency analysis was divided between the E) upper, papillary dermis, and F) lower, reticular dermis.

#### Skin deformation and growth

Surfaces for each of the time points of the protocol were reconstructed for each of four XRTE patches and one TE patch treated as control for this analysis. Surface reconstruction is shown in Fig. 5A for one of the patches, where it can be appreciated how the tattooed grid on the animal gets deformed due to inflation of the expander up to the point immediate before animal sacrifice. The deformation from the pre-inflation 1 to just prior to sacrifice is  $\mathbf{F}(t)$ . Post-sacrifice, the skin is excised and it contracts releasing the elastic deformation  $\mathbf{F}^e$ . If the

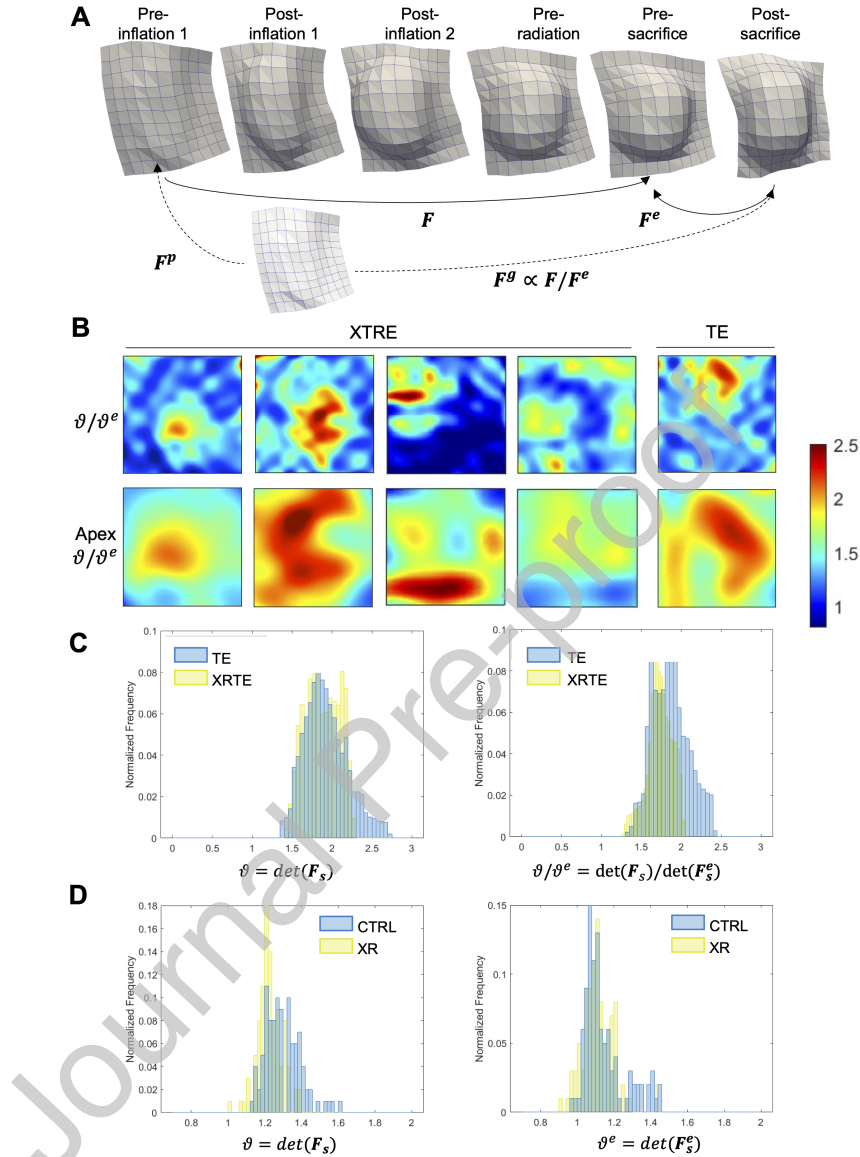


Figure 5: IGA analysis of skin growth. A) Reconstructed surfaces from 3D photos were available for each step of the protocol. Starting from the initial in vivo state before expansion, up to the in vivo tissue before sacrifice, the deformation is denoted  $\mathbf{F}$ . Excised tissue after animal sacrifice shrinks, revealing that not all the deformation seen in vivo is growth but rather there is some elastic deformation  $\mathbf{F}^e$ . Skin in vivo at the start of the protocol is already pre-stressed by some unobserved amount  $\mathbf{F}^p$ . Growth is thus proportional to  $\mathbf{F} \propto \mathbf{F}\mathbf{F}^{e-1}$ , with the proportionality depending on the existing  $\mathbf{F}^p$  before expansion. B) Contours of area change  $\vartheta/\vartheta^e$ , with  $\vartheta = \det(\mathbf{F}_s)$ ,  $\vartheta^e = \det(\mathbf{F}_s^e)$ , reveal that the expander apex is the region with most growth. The results are similar between XRTE and TE. C) Histogram of growth distribution shows a shift toward lower growth values in XRTE compared to TE but we could not assess significance. Nevertheless, this analysis, together with XRTE showing the same thickness as controls, indicates that skin is indeed growing in the XRTE case. D) Comparison between CTRL and XR patches shows that radiated skin shrinks in vivo with respect to CTRL over 8 weeks after radiation. Excision at the end of the 8 weeks reveals a small shift in the XR case toward smaller elastic deformation compared to CTRL. In other words, radiated skin shows less elastic recoil upon excision.

290 pre-inflation skin patch was extracted it would contract revealing the pre-stretch  $\mathbf{F}^p$ . However, this configuration is not available. Growth or permanent deformation  $\mathbf{F}^g$  maps from the stress free intermediate configuration to the post-sacrifice geometry. Because we do not have the pre-stretch, we can only compute permanent deformation up to a scaling factor  $\mathbf{F}^g \propto \mathbf{F}\mathbf{F}^{-1}$ . The contours of the deformation  $\vartheta/\vartheta^e$  (only area change) are shown in Fig. 5B. Note that the 295 contours are plotted over the same unit square for easy of comparison, but these are contours over the surfaces of Fig. 5A. The expander can be clearly identified in the contours Fig. 5B as the region with greatest deformation. The region at the apex of the expander is further zoomed in to show range of deformation. Based on the contours alone there is little difference between the expanded radiated and expanded patches. The histograms of Fig. 5C further show the 300 distribution of the total deformation and the plastic deformation  $\vartheta/\vartheta^e$ . The initial deformation is similar between all patches, with the permanent deformation or growth reaching higher values in the TE case compared to the XRTE case. The area change of XRTE due to growth has median  $\vartheta/\vartheta^e = 1.72$ , while for TE case it is  $\vartheta/\vartheta^e = 1.85$ . To provide an indication of variability in the histogram of Fig. 5C, the 10<sup>th</sup> percentile of  $\vartheta/\vartheta^e$  is 1.41 and 1.58 respectively for XRTE and TE. The 90<sup>th</sup> percentile is 2.05 and 2.19 for XRTE and TE. Given that thickness increased in XRTE compared to CTRL, these data suggest that XRTE tissue is still able to growth under expansion, but not as much as TE tissues. Fig. 5D shows the comparison between a CTRL and a XR patches. The in vivo deformation for CTRL skin is expected to be slightly greater than one because of natural growth of the pig. The 90% confidence interval for in vivo  $\vartheta$  for the 305 CTRL patch is [1.18, 1.44]. The XR patch shows a histogram shift to the left for  $\vartheta$ , with a 90% confidence interval [1.14, 1.32], indicative of in vivo contraction 8 weeks after radiation. Furthermore, when excising the skin, the CTRL patch reveals a slightly greater elastic 310 deformation compared to XR. For the CTRL patch, the 90% confidence interval for  $\vartheta^e$  is [1.0, 1.35]. For the XR patch, the 90% confidence interval for  $\vartheta^e$  shifts to the left [1.0, 1.23].

315

## Discussion

320 Radiated groups, XR and XRTE, are stiffer than normal skin when compared at lower deformations, based on a significant reduction of the transition stretch compared to controls. For the high stiffness region, XR showed a clear increase in the modulus compared to CTRL and, interestingly, XRTE was not significantly different from CTRL. The changes in mechanical properties are driven by collagen structure changes such as bundle formation which is reflected in the reduced dispersion of the orientation distributions in the XR and XRTE skin compared to 325 controls, with XR showing the most concentrated fiber orientation. The coherency metric, which also quantifies the strength of collagen alignment, shows contrasting results between the upper and lower dermis. In the UD, coherency values were overall lower than in the LD region and XRTE showed higher coherency. The LD region showed that XR achieved the highest coherency and XRTE the lowest.

330 It is well-known that radiation contributes to tissue fibrosis [61, 62, 63]. Here we add to that existing knowledge by showing that tissue expansion counteracts some of the fibrotic response seen after radiation treatment. XRTE samples still showed increased stiffness compared to controls in some metrics, namely the transition stretch, but to a lesser extent than XR samples. For the high modulus, XR showed, as expected, the highest value in the dorsal-ventral direction which is aligned with the preferred fiber orientation, while XRTE was not different from controls. Collagen analysis also showed that XRTE looked more similar to controls than to the XR group. These results suggest that TE and XR have opposing roles in collagen remodeling.

335 The hierarchical collagen fiber structure together with the presence of intra-fibrillar and  
 inter-fibrillar cross-links, are key determinants of skin mechanical behavior at the macroscale  
 [64, 65, 42]. Upon radiation, there are multiple mechanisms contributing to fibrosis over several  
 time scales. Direct damage and cleavage of fiber bundles together with formation of new  
 cross-links are immediate effects of radiation [26, 66]. Radiation injury to epithelial and  
 340 endothelial cells triggers sterile inflammation that activates a pro-fibrotic response by resident  
 fibroblast cells on longer time scales (4 to 6 weeks) [67, 21]. Here we evaluated the longer time  
 scale, 8 weeks after radiation. Previous reports looking at collagen remodeling through atomic  
 force microscopy (AFM) imaging and scanning electronic micrographs (SEM) reported  
 collagen disorganization and thinning of fibers approximately one month after radiation  
 345 [24, 67]. Histological staining has showed increased thickness and overall collagen content over  
 2 and 4 months following slightly higher doses of radiation to what we show here [68]. The  
 analysis showed here based on OrientationJ has been used for normal skin characterization but  
 not in the context of RIF [58, 45]. We did not observe thinner collagen fibers but rather thick  
 350 collagen structures (Fig. 4), reflected in the coherency metric [54]. One explanation for the  
 discrepancy regarding thinner fibers reported in the literature but not found here is the difference  
 in spatial and temporal scales of the analyses. Radiation leads to acute collagen fiber  
 fragmentation that can be appreciated in AFM and SEM techniques, whereas histology captures  
 collagen distribution at the scale of the entire tissue thickness. Thus, our analysis shows  
 355 changes in collagen fiber bundles rather than the geometry of individual fibers. Histology  
 images here do coincide with previous work in the RIF literature, especially on the longer time  
 scales of 8 weeks or more [68]. The authors in [68] report evidence of fibrosis in the histology  
 images based on the increase in epidermal and dermal thickness. In our study, while the  
 360 epidermal thickness exhibits relatively minor fluctuations, the overall thickness of XR skin  
 samples was indeed the highest. Thus, even if acutely there could be some direct damage to  
 collagen structure, chronic inflammation, possibly through sustained TGF $\beta$ 1 expression [69],  
 can explain increased collagen production and fibrosis as seen here. Notably, the changes in  
 coherency were depth dependent. The greatest changes were observed in the LD. Megavoltage  
 365 photon beams, characterized by their high-energy nature, can penetrate deeply into tissue  
 [70, 71]. This mechanism can minimize radiation exposure to superficial tissues such as the  
 skin surface [70], providing insight into the depth-dependence observed in our findings.  
 With respect to the effect of TE, we have shown in our previous work, with similar analysis  
 techniques as in the present paper, that TE leads to collagen fiber disorganization measured as a  
 370 decrease in coherency and a greater fiber dispersion compared to controls [59]. Gene expression  
 analysis has further showed upregulation of matrix metalloproteinases (MMPs) in TE,  
 explaining the collagen disorganization [6]. Others have also reported softening of skin with TE  
 and fiber network disorganization [72, 73].  
 Together, our results suggest that TE counteracts some of the fibrotic effects of radiation by  
 375 promoting collagen remodeling. However, the nonlinear nature of skin biomechanics suggests a  
 nuanced approach [42]. Even though XR showed the highest modulus and there was no  
 significant difference between XRTE and CTRL, in other metrics such as the transition stretch,  
 both XRTE and XR were different to CTRL. Nevertheless, XR was still the one with the  
 greatest indication of fibrosis (Fig. 2), aligning with previous reports on XR tissues [62]. In  
 previous work, we have shown that the transition stretch might be also an important metric to  
 characterize loosening of skin with age [74, 58]. Thus, we advocate for reporting at least low  
 380 and high moduli as well as transition stretches [74, 58].  
 The IGA analysis allowed us to test if TE leads to permanent area growth even in the presence

of radiation. We confirmed that there is permanent deformation in XRTE but it was lower with respect to the TE patch we had as control in this case. We attributed the permanent area change to growth because the area changes occurred with an increase in thickness, i.e. there was a net increase in tissue volume. Thus, our experiments suggest that indeed TE is promoting tissue regeneration even in the presence of radiation, which helps explains the collagen analysis.

#### *Limitations and future work*

One limitation is the amount of data available. More experiments would be beneficial to increase statistical power. This would also allow us to investigate the effect of possible anterior-posterior changes in skin mechanics which were not considered in this study. The porcine protocol is robust but complications do occur. For instance, we lost one TE patch due to expander leakage. As a result, while we can state that skin grew in the XRTE case, the comparison against TE is qualitative since we only had one TE patch to compare against. Additionally, for one the XRTE patches a lower volume was administered for concerns of skin viability. The Supplement shows the results excluding this XRTE patch but the conclusions remain the same.

We are continuing this line of investigation to better characterize XR and TE effects on porcine skin. The focus on this manuscript is the mechanical response of the tissue. We know from previous work that TE induces specific proliferative processes [6]. We also know from previous work in the literature that radiation induces endothelial cell damage, ROS, sterile inflammation, and pro-fibrotic fibroblast phenotype [37]. Thus, a clear step of future work is a much more detail quantification of these biological processes in the combined XR+TE. While we relate changes in skin stiffness to variations in collagen distribution, our study did not assess tissue contraction in detail, which could provide additional insights into the observed alterations in mechanical properties such as the transition stretch. Contraction is associated with myofibroblast activity following radiation-induced injury [75]. IGA analysis revealed contraction of the XR patch relative to CTRL (Fig. 5), but we did not measure this deformation in all patches.

Clinically, the present study suggests that PMRT immediately after TE, or delayed-immediate reconstruction, could reduce negative effects of radiation such as RIF. There is indeed a trend to perform immediate reconstruction or immediate-delayed reconstruction with TE in conjunction with PMRT [14, 76, 20]. On the one hand, there is higher rate of complications requiring surgical intervention when the expander is radiated compared to the implant [16, 9]. On the other hand, radiation to the permanent implant (after completion of the final reconstructive procedure), leads to greater incidence of RIF and poor cosmetic outcomes [16, 17]. This is in line with our study, with radiation to the expander being similar to our XRTE protocol, and radiation to the permanent implant captured with our XR patches. Some of the increase in immediate reconstruction followed by PMRT is explained by innovations in devices and surgical technique, e.g. the use of biological cover, which we have investigated recently [32, 77]. Topical treatments to reduce RIF in the skin have also emerged, most notably deferoxamine [37]. Ultimately, it is clear that there is still a lack of scientific understanding around TE and PMRT.

#### Conclusion

Radiation induces skin stiffening due to collagen production and reorganization over the course of several weeks. Tissue expansion, on the other hand, is known to induce pro-regenerative

pathways that also remodel collagen, inducing acute softening but ultimately creating tissue with the same characteristics as the original, healthy skin. We were interested in the interplay between TE and XR because both are typical for breast reconstruction after mastectomy. We showed that TE immediately after radiation counteracts some of the negative effects of radiation , specifically RIF. We anticipate that this study will guide future characterization of biology in the presence of XR and TE to further understand how TE can counteract XR effects and to better leverage these mechanisms in new therapeutic strategies involving radiation.

### Author Contributions

LNA conducted the mechanical tests, analyzed the data, wrote the paper. VT helped with Bayesian calibration analysis. JL, SA, BP collected and processed tissue samples, processed histology, acquired 3D photographs. TH and JL did the IGA analysis. AG supervised all porcine experiments. ABT supervised all the data analysis and wrote the paper.

### Acknowledgments

ABT acknowledges support from the National Institute of Arthritis and Musculoskeletal and Skin Diseases, National Institute of Health, United States under award R01AR074525. Additional support was provided by the PSF/MTF Biologics Allograft Tissue Research Grant 2018PSF000MTF/ PS0176133 and the PSF/ MTF Biologics Allograft Tissue Research Grant 2022PSF000MTF/ PS0238098.

### Supplementary Material

The Bayesian calibration code can be found at  
[https://github.com/abuganza/RadiationTE\\_R2](https://github.com/abuganza/RadiationTE_R2).

### References

- [1] A. N. Giaquinto, H. Sung, K. D. Miller, J. L. Kramer, L. A. Newman, A. Minihan, A. Jemal, R. L. Siegel, Breast cancer statistics, 2022, CA: a cancer journal for clinicians 72 (6) (2022) 524–541.
- [2] K. L. Kummerow, L. Du, D. F. Penson, Y. Shyr, M. A. Hooks, Nationwide trends in mastectomy for early-stage breast cancer, JAMA surgery 150 (1) (2015) 9–16.
- [3] T. M. Johnson, L. Lowe, M. D. Brown, M. J. Sullivan, B. R. Nelson, Histology and physiology of tissue expansion, The Journal of dermatologic surgery and oncology 19 (12) (1993) 1074–1078.
- [4] J. Marcus, D. B. Horan, J. K. Robinson, Tissue expansion: past, present, and future, Journal of the American Academy of Dermatology 23 (5) (1990) 813–825.
- [5] K. D. Miller, L. Nogueira, A. B. Mariotto, J. H. Rowland, K. R. Yabroff, C. M. Alfano, A. Jemal, J. L. Kramer, R. L. Siegel, Cancer treatment and survivorship statistics, 2019, CA: a cancer journal for clinicians 69 (5) (2019) 363–385.
- [6] J. K. Ledwon, L. J. Kelsey, E. E. Vaca, A. K. Gosain, Transcriptomic analysis reveals dynamic molecular changes in skin induced by mechanical forces secondary to tissue expansion, Scientific reports 10 (1) (2020) 15991.
- [7] L. E. Janes, J. K. Ledwon, E. E. Vaca, S. Y. Turin, T. Lee, A. B. Tepole, H. Bae, A. K. Gosain, Modeling tissue expansion with isogeometric analysis: skin growth and tissue level changes in the porcine model, Plastic and reconstructive surgery 146 (4) (2020) 792–798.
- [8] R. Jaggi, J. Jiang, A. O. Momoh, A. Alderman, S. H. Giordano, T. A. Buchholz, L. J. Pierce, S. J. Kronowitz, B. D. Smith, Complications after mastectomy and immediate breast reconstruction for breast cancer: a claims-based analysis, Annals of surgery 263 (2) (2016) 219–227.

- [9] C. J. Anker, R. V. Hymas, R. Ahluwalia, K. E. Kokeny, V. Avizonis, K. M. Boucher, L. A. Neumayer, J. P. Agarwal, The effect of radiation on complication rates and patient satisfaction in breast reconstruction using temporary tissue expanders and permanent implants, *The breast journal* 21 (3) (2015) 233–240.
- 470 [10] L. L. Frasier, S. Holden, T. Holden, J. R. Schumacher, G. Leverson, B. Anderson, C. C. Greenberg, H. B. Neuman, Temporal trends in postmastectomy radiation therapy and breast reconstruction associated with changes in national comprehensive cancer network guidelines, *JAMA oncology* 2 (1) (2016) 95–101.
- [11] S. A. Chen, C. Hiley, D. Nickleach, J. Petsuksiri, F. Andic, O. Riesterer, J. M. Switchenko, M. A. Torres, Breast reconstruction and post-mastectomy radiation practice, *Radiation Oncology* 8 (2013) 1–9.
- 475 [12] L. A. Stevens, M. H. McGrath, R. G. Druss, S. J. Kister, F. E. Gump, K. A. Forde, The psychological impact of immediate breast reconstruction for women with early breast cancer, *Plastic and Reconstructive Surgery* 73 (4) (1984) 619–626.
- [13] E. E. Elder, Y. Brandberg, T. Björklund, R. Rylander, J. Lagergren, G. Jurell, M. Wickman, K. Sandelin, Quality of life and patient satisfaction in breast cancer patients after immediate breast reconstruction: a prospective study, *The breast* 14 (3) (2005) 201–208.
- 480 [14] A. Y. Ho, Z. I. Hu, B. J. Mehrara, E. G. Wilkins, Radiotherapy in the setting of breast reconstruction: types, techniques, and timing, *The Lancet Oncology* 18 (12) (2017) e742–e753.
- [15] S. Agarwal, K. M. Kidwell, A. Farberg, J. H. Kozlow, K. C. Chung, A. O. Momoh, Immediate reconstruction of the radiated breast: recent trends contrary to traditional standards, *Annals of surgical oncology* 22 (2015) 2551–2559.
- 485 [16] A. F. Mericli, S. E. Sharabi, Breast implants and radiation, in: *Seminars in Plastic Surgery*, Vol. 33, Thieme Medical Publishers, 2019, pp. 240–246.
- [17] P. R. Anderson, A. L. Hanlon, S. W. McNeeley, G. M. Freedman, Low complication rates are achievable after post-mastectomy breast reconstruction and radiation therapy, *International Journal of Radiation Oncology\* Biology\* Physics* 59 (4) (2004) 1080–1087.
- 490 [18] P. G. Cordeiro, C. R. Albornoz, B. McCormick, Q. Hu, K. Van Zee, The impact of postmastectomy radiotherapy on two-stage implant breast reconstruction: an analysis of long-term surgical outcomes, aesthetic results, and satisfaction over 13 years, *Plastic and reconstructive surgery* 134 (4) (2014) 588–595.
- [19] S. J. Kronowitz, K. K. Hunt, H. M. Kuerer, G. Babiera, M. D. McNeese, T. A. Buchholz, E. A. Strom, G. L. Robb, Delayed-immediate breast reconstruction, *Plastic and reconstructive surgery* 113 (6) (2004) 1617–1628.
- 495 [20] H. Ryu, K. H. Shin, J. H. Chang, B.-S. Jang, A nationwide study of breast reconstruction after mastectomy in patients with breast cancer receiving postmastectomy radiotherapy: comparison of complications according to radiotherapy fractionation and reconstruction procedures, *British Journal of Cancer* (2024) 1–9.
- [21] M. R. Borrelli, A. H. Shen, G. K. Lee, A. Momeni, M. T. Longaker, D. C. Wan, Radiation-induced skin fibrosis: pathogenesis, current treatment options, and emerging therapeutics, *Annals of plastic surgery* 83 (2019) S59. doi:10.1097/SAP.000000000002098.
- 500 URL <https://www.ncbi.nlm.nih.gov/pmc/articles/PMC6746243/>?report=abstracthttps://www.ncbi.nlm.nih.gov/pmc/articles/PMC6746243/
- [22] M. Martin, J. L. Lefait, S. Delanian, Tgf-b1 and radiation fibrosis: A master switch and a specific therapeutic target?, *International Journal of Radiation Oncology Biology Physics* 47 (2000) 277–290. doi:10.1016/S0360-3016(00)00435-1.
- 505 URL <https://pubmed.ncbi.nlm.nih.gov/10802350/>
- [23] O. Krysko, T. L. Aaes, C. Bachert, P. Vandeneabeele, D. V. Krysko, Many faces of damps in cancer therapy, *Cell Death Disease* 2013 4:5 4 (2013) e631–e631. doi:10.1038/cddis.2013.156.
- 510 URL <https://www.nature.com/articles/cddis2013156>
- [24] C. B. V. de Andrade, I. P. R. Ramos, A. C. N. de Moraes, A. L. R. do Nascimento, C. Salata, R. C. d. S. Goldenberg, J. J. de Carvalho, C. E. V. de Almeida, Radiotherapy-induced skin reactions induce fibrosis mediated by tgf- $\beta$ 1 cytokine, *Dose-Response* 15 (2) (2017) 1559325817705019.
- [25] E. Balli, U. Comelekoglu, E. Yalin, N. Yilmaz, S. Aslantas, F. Sgt, M. Berkz, S. Yalin, Exposure to gamma rays induces early alterations in skin in rodents: Mechanical, biochemical and structural responses, *Ecotoxicology and Environmental Safety* 72 (2009) 889–894. doi:10.1016/J.ECOENV.2008.09.021.
- 515 [26] A. Maslennikova, M. Kochueva, N. Ignatieva, A. Vitkin, O. Zakharkina, V. Kamensky, E. Sergeeva, E. Kiseleva, V. Bagratashvili, Effects of gamma irradiation on collagen damage and remodeling, *International journal of radiation biology* 91 (2015) 240–247. doi:10.3109/09553002.2014.969848.
- URL <https://pubmed.ncbi.nlm.nih.gov/25300691/>
- [27] X. Liang, X. Huang, Y. Zhou, R. Jin, Q. Li, Mechanical stretching promotes skin tissue regeneration via enhancing mesenchymal stem cell homing and transdifferentiation, *Stem cells translational medicine* 5 (2016) 960–969. doi:10.5966/SCTM.2015-0274.
- 520 URL <https://pubmed.ncbi.nlm.nih.gov/27130223/>
- [28] M. S. Chin, R. Ogawa, L. Lancerotto, G. Pietramaggiore, K. T. Schomacker, J. C. Mathews, S. S. Scherer, P. Van Duyn, M. J. Prsa, M. P. Ottensmeyer, et al., In vivo acceleration of skin growth using a servo-controlled

- stretching device, *Tissue Engineering Part C: Methods* 16 (3) (2010) 397–405.
- [29] A. Summerfield, F. Meurens, M. E. Ricklin, The immunology of the porcine skin and its value as a model for human skin, *Molecular Immunology* 66 (2015) 14–21. doi:10.1016/J.MOLIMM.2014.10.023.
- [30] T. P. Sullivan, W. H. Eaglstein, S. C. Davis, P. Mertz, The pig as a model for human wound healing, *Wound Repair and Regeneration* 9 (2001) 66–76. doi:10.1046/J.1524-475X.2001.00066.X.  
 URL <https://onlinelibrary.wiley.com/doi/full/10.1046/j.1524-475x.2001.00066.x>  
<https://onlinelibrary.wiley.com/doi/abs/10.1046/j.1524-475x.2001.00066.x>  
<https://onlinelibrary.wiley.com/doi/10.1046/j.1524-475x.2001.00066.x>
- [31] F. Meurens, A. Summerfield, H. Nauwynck, L. Saif, V. Gerdts, The pig: a model for human infectious diseases, *Trends in Microbiology* 20 (2012) 50–57. doi:10.1016/J.TIM.2011.11.002.
- [32] J. K. Ledwon, S. A. Applebaum, B. Progris, O. Vignesh, K. S. Gutowski, A. B. Chang, A. B. Tepole, A. K. Gosain, Biological cover mitigates disruption of the dermal structure in mechanically expanded skin in a porcine model, *International journal of molecular sciences* 23 (21) (2022) 13091.
- [33] A. B. Tepole, E. E. Vaca, C. A. Purnell, M. Gart, J. McGrath, E. Kuhl, A. K. Gosain, Quantification of strain in a porcine model of skin expansion using multi-view stereo and isogeometric kinematics, *JoVE (Journal of Visualized Experiments)* (122) (2017) e55052.
- [34] I. Hadad, B. H. Johnstone, J. G. Brabham, M. W. Blanton, P. I. Rogers, C. Fellers, J. L. Solomon, S. Merfeld-Clauss, C. M. DesRosiers, J. R. Dynlacht, et al., Development of a porcine delayed wound-healing model and its use in testing a novel cell-based therapy, *International Journal of Radiation Oncology\* Biology\* Physics* 78 (3) (2010) 888–896.
- [35] J. O. Archambeau, A. Ines, L. F. Fajardo, Response of swine skin microvasculature to acute single exposures of x rays: quantification of endothelial changes, *Radiation research* 98 (1) (1984) 37–51.
- [36] M. Barton, Tables of equivalent dose in 2 gy fractions: A simple application of the linear quadratic formula, *International Journal of Radiation Oncology Biology Physics* 31 (1995) 371–378. doi:10.1016/0360-3016(94)E0126-5.
- [37] A. H. Shen, M. R. Borrelli, S. Adem, N. M. Deleon, R. A. Patel, S. Mascharak, S. J. Yen, B. Y. Sun, W. L. Taylor, M. Januszyk, D. H. Nguyen, A. Momeni, G. C. Gurther, M. T. Longaker, D. C. Wan, Prophylactic treatment with transdermal deferoxamine mitigates radiation-induced skin fibrosis, *Scientific reports* 10 (12 2020). doi:10.1038/S41598-020-69293-4.  
 URL <https://pubmed.ncbi.nlm.nih.gov/32704071/>
- [38] J. T. Tubon, V. D. Sree, J. Payne, L. Solorio, A. B. Tepole, Mechanical damage in porcine dermis: Micro-mechanical model and experimental characterization, *Journal of the Mechanical Behavior of Biomedical Materials* 147 (2023) 106143.
- [39] T. Han, T. Lee, J. Ledwon, E. Vaca, S. Turin, A. Kearney, A. K. Gosain, A. B. Tepole, Bayesian calibration of a computational model of tissue expansion based on a porcine animal model, *Acta biomaterialia* 137 (2022) 136–146.
- [40] V. Tac, V. D. Sree, M. K. Rausch, A. B. Tepole, Data-driven modeling of the mechanical behavior of anisotropic soft biological tissue, *Engineering with Computers* 38 (5) (2022) 4167–4182.
- [41] K. Linka, A. B. Tepole, G. A. Holzapfel, E. Kuhl, Automated model discovery for skin: Discovering the best model, data, and experiment, *Computer Methods in Applied Mechanics and Engineering* 410 (2023) 116007.
- [42] J. W. Jor, M. P. Nash, P. M. Nielsen, P. J. Hunter, Estimating material parameters of a structurally based constitutive relation for skin mechanics, *Biomechanics and modeling in mechanobiology* 10 (5) (2011) 767–778.
- [43] G. A. Holzapfel, T. C. Gasser, R. W. Ogden, A new constitutive framework for arterial wall mechanics and a comparative study of material models, *Journal of elasticity and the physical science of solids* 61 (2000) 1–48.
- [44] T. C. Gasser, R. W. Ogden, G. A. Holzapfel, Hyperelastic modelling of arterial layers with distributed collagen fibre orientations, *Journal of the royal society interface* 3 (6) (2006) 15–35.
- [45] A. Ní Annaidh, K. Bruyère, M. Destrade, M. D. Gilchrist, C. Maurini, M. Otténio, G. Saccomandi, Automated estimation of collagen fibre dispersion in the dermis and its contribution to the anisotropic behaviour of skin, *Annals of biomedical engineering* 40 (8) (2012) 1666–1678.
- [46] A. N. Annaidh, M. Destrade, Tension lines of the skin, *Skin Biophysics: From Experimental Characterisation to Advanced Modelling* (2019) 265–280.
- [47] S. Chen, A. Ní Annaidh, S. Roccabianca, A microstructurally inspired constitutive model for skin mechanics, *Biomechanics and modeling in mechanobiology* 19 (2020) 275–289.
- [48] S. Jaiswal, R. Hannineh, S. Nadimpalli, S. Lieber, S. A. Chester, Characterization and modeling of the in-plane collagen fiber distribution in the porcine dermis, *Medical Engineering & Physics* 115 (2023) 103973.
- [49] G. Limbert, Constitutive modelling of skin mechanics, in: *Skin Biophysics*, Springer, 2019, pp. 19–76.
- [50] M. Rausch, W. D. Meador, J. Toaquiza-Tubon, O. Moreno-Flores, A. B. Tepole, Biaxial mechanics of thermally denaturing skin-part 2: Modeling, *Acta biomaterialia* 140 (2022) 421–433.
- [51] T. K. Tonge, L. M. Voo, T. D. Nguyen, Full-field bulge test for planar anisotropic tissues: Part ii—a thin shell method for determining material parameters and comparison of two distributed fiber modeling approaches, *Acta*

- 585 biomaterialia 9 (4) (2013) 5926–5942.
- [52] M. Pensalfini, A. B. Tepole, Mechano-biological and bio-mechanical pathways in cutaneous wound healing, *PLoS computational biology* 19 (3) (2023) e1010902.
- [53] D. Phan, N. Pradhan, M. Jankowiak, Composable effects for flexible and accelerated probabilistic programming in numpyro, *arXiv preprint arXiv:1912.11554* (2019).
- 590 [54] R. Rezakhanlou, A. Agianniotis, J. T. C. Schrauwen, A. Griffa, D. Sage, C. v. Bouting, F. Van De Vosse, M. Unser, N. Stergiopoulos, Experimental investigation of collagen waviness and orientation in the arterial adventitia using confocal laser scanning microscopy, *Biomechanics and modeling in mechanobiology* 11 (2012) 461–473.
- [55] T. Clemons, M. Bradshaw, P. Toshniwal, N. Chaudhari, A. Stevenson, J. Lynch, M. Fear, F. Wood, K. S. Iyer, Coherency image analysis to quantify collagen architecture: implications in scar assessment, *RSC advances* 8 (18) (2018) 9661–9669.
- 595 [56] A. B. Tepole, M. Gart, A. K. Gosain, E. Kuhl, Characterization of living skin using multi-view stereo and isogeometric analysis, *Acta biomaterialia* 10 (11) (2014) 4822–4831.
- [57] M. Kwak, D. Son, J. Kim, K. Han, Static Langer's line and wound contraction rates according to anatomical regions in a porcine model, *Wound Repair and Regeneration* 22 (5) (2014) 678–682.
- 600 [58] W. D. Meador, G. P. Sugerman, H. M. Story, A. W. Seifert, M. R. Bersi, A. B. Tepole, M. K. Rausch, The regional-dependent biaxial behavior of young and aged mouse skin: A detailed histomechanical characterization, residual strain analysis, and constitutive model, *Acta biomaterialia* 101 (2020) 403–413.
- [59] T. Lee, E. E. Vaca, J. K. Ledwon, H. Bae, J. M. Topczewska, S. Y. Turin, E. Kuhl, A. K. Gosain, A. B. Tepole, Improving tissue expansion protocols through computational modeling, *Journal of the mechanical behavior of biomedical materials* 82 (2018) 224–234.
- 605 [60] V. Sivan, M.-C. Vozenin-Brottons, Y. Tricaud, J.-L. Lefait, J.-M. Cossat, B. Dubray, M. T. Martin, Altered proliferation and differentiation of human epidermis in cases of skin fibrosis after radiotherapy, *International Journal of Radiation Oncology\* Biology\* Physics* 53 (2) (2002) 385–393.
- [61] S. Delanian, J.-L. Lefait, The radiation-induced fibrotrophic process: therapeutic perspective via the antioxidant pathway, *Radiotherapy and oncology* 73 (2) (2004) 119–131.
- 610 [62] N.-T. A. Nguyen, D. Roberge, C. R. Freeman, C. Wong, J. Hines, R. E. Turcotte, Skin elasticity as a measure of radiation fibrosis: is it reproducible and does it correlate with patient and physician-reported measures?, *Technology in cancer research & treatment* 13 (5) (2014) 469–476.
- [63] B. M. Zwaans, M. Grobbel, A. L. Carabalea, L. E. Lamb, S. Roccabianca, Increased extracellular matrix stiffness accompanies compromised bladder function in a murine model of radiation cystitis, *Acta biomaterialia* 144 (2022) 221–229.
- 615 [64] Y. Lanir, A structural theory for the homogeneous biaxial stress-strain relationships in flat collagenous tissues, *Journal of biomechanics* 12 (6) (1979) 423–436.
- [65] W. Kong, C. Lyu, H. Liao, Y. Du, Collagen crosslinking: effect on structure, mechanics and fibrosis progression, *Biomedical Materials* 16 (6) (2021) 062005.
- 620 [66] A. Ittycheri, Z. W. Lipsky, T. A. Hookway, G. K. German, Ultraviolet light induces mechanical and structural changes in full thickness human skin, *Journal of the Mechanical Behavior of Biomedical Materials* 143 (2023) 105880.
- [67] A. O. Luby, A. E. Snider, G. S. Mandair, K. M. Urlaub, J. V. Lynn, N. S. Nelson, A. Donneys, R. E. Ettinger, G. C. Gurtner, D. Kohn, et al., Therapeutic interventions to reduce radiation induced dermal injury in a murine model of tissue expander based breast reconstruction, *Annals of plastic surgery* 85 (5) (2020) 546.
- 625 [68] J. A. Horton, E. J. Chung, K. E. Hudak, A. Sowers, A. Thetford, A. O. White, J. B. Mitchell, D. E. Citrin, Inhibition of radiation-induced skin fibrosis with imatinib, *International journal of radiation biology* 89 (3) (2013) 162–170.
- [69] J. Hopewell, The skin: its structure and response to ionizing radiation, *International journal of radiation biology* 57 (4) (1990) 751–773.
- 630 [70] E. B. Podgorsak, et al., Review of radiation oncology physics: a handbook for teachers and students, Vienna, Austria: IAE Agency 19 (2003) 133.
- [71] R. Sjögren, M. G. Karlsson, M. Karlsson, H. Svensson, Depth for dose calibration in high energy photon beams, *Radiotherapy and oncology* 43 (3) (1997) 311–313.
- 635 [72] E. J. Timmenga, R. Schoorl, P. J. Klopper, Biomechanical and histomorphological changes in expanded rabbit skin, *British journal of plastic surgery* 43 (1) (1990) 101–106.
- [73] N. A. S. Manssor, Z. Radzi, N. A. Yahya, L. Mohamad Yusof, F. Hariri, N. H. Khairuddin, N. H. Abu Kasim, J. T. Czernuska, Characteristics and young's modulus of collagen fibrils from expanded skin using anisotropic controlled rate self-inflating tissue expander, *Skin pharmacology and physiology* 29 (2) (2016) 55–62.
- 640 [74] C.-Y. Lin, G. P. Sugerman, S. Kakaltsis, W. D. Meador, A. T. Buganza, M. K. Rausch, Sex-and age-dependent skin mechanics a detailed look in mice, *Acta Biomaterialia* 175 (2024) 106–113.
- [75] S. Kulshrestha, R. Chawla, S. Singh, P. Yadav, N. Sharma, R. Goel, H. Ojha, V. Kumar, J. Adhikari, Protection of sildenafil citrate hydrogel against radiation-induced skin wounds, *Burns* 46 (5) (2020) 1157–1169.

- 645 [76] S. N. Razdan, P. G. Cordeiro, C. R. Albornoz, J. J. Disa, H. J. Panchal, A. Y. Ho, A. O. Momoh, E. Matros, National breast reconstruction utilization in the setting of postmastectomy radiotherapy, *Journal of reconstructive microsurgery* 33 (05) (2017) 312–317.
- [77] J. K. Ledwon, S. A. Applebaum, B. Progri, T. Han, O. Vignesh, K. S. Gutowski, A. B. Chang, N. K. Reddy, A. B. Tepole, A. K. Gosain, Acellular dermal matrix cover improves skin growth during tissue expansion by affecting distribution of mechanical forces, *Plastic and reconstructive surgery* 153 (4) (2024) 663e–672e.

**Statement of significance**

Breast cancer is the most prevalent in women and its treatment often results in total breast removal (mastectomy), followed by reconstruction using tissue expanders. Radiation, which is used in about a third of breast reconstruction cases, can lead to significant complications. The timing of radiation treatment remains controversial. Radiation is known to cause immediate skin damage and long-term fibrosis. Tissue expansion leads to a pro-regenerative response involving collagen remodeling. Here we show that tissue expansion immediately prior to radiation can reduce the level of radiation-induced fibrosis. Thus, we anticipate that this new evidence will open up new avenues of investigation into how the collagen remodeling and pro-regenerative effects of tissue expansion can be leverage to prevent radiation-induced fibrosis.

**Declaration of interests**

- The authors declare that they have no known competing financial interests or personal relationships that could have appeared to influence the work reported in this paper.
- The author is an Editorial Board Member/Editor-in-Chief/Associate Editor/Guest Editor for *ASME Journal of Biomechanical Engineering* and was not involved in the editorial review or the decision to publish this article.
- The authors declare the following financial interests/personal relationships which may be considered as potential competing interests:



A large, empty rectangular box with a thin black border, intended for the author to list any potential competing interests.